



Original article

Crystal structures, antioxidation and DNA binding properties of Dy(III) complexes with Schiff-base ligands derived from 8-hydroxyquinoline-2-carboxaldehyde and four aroylhydrazines

Yong-chun Liu^{a,b}, Zheng-yin Yang^{a,*}^a College of Chemistry and Chemical Engineering, State Key Laboratory of Applied Organic Chemistry, Lanzhou University, Lanzhou 730000, PR China^b College of Chemistry and Chemical Engineering, Longdong University, Qingyang, Gansu 745000, PR China

ARTICLE INFO

Article history:

Received 1 January 2009

Received in revised form

13 August 2009

Accepted 10 September 2009

Available online 16 September 2009

Keywords:

Rare earths

Schiff bases

X-ray crystallography

Calf thymus DNA binding properties

Antioxidation

ABSTRACT

X-ray crystal and other structural analyses indicate that Dy(III) and every ligand can form a binuclear Dy(III) complex with nine-coordination and 1:1 metal-to-ligand stoichiometry at the Dy(III) center. All the ligands and Dy(III) complexes can bind to Calf thymus DNA through intercalations with the binding constants at the order of magnitude 10^5 – 10^7 M⁻¹, but Dy(III) complexes present stronger affinities to DNA than ligands. All the ligands and Dy(III) complexes can be used as potential anticancer drugs. All the ligands and Dy(III) complexes have strong scavenging effects for hydroxyl radicals and superoxide radicals but complex containing active phenolic hydroxyl group shows stronger scavenging effects for hydroxyl radicals and complex containing *N*-heteroaromatic substituent shows stronger scavenging effects for superoxide radicals.

© 2009 Elsevier Masson SAS. All rights reserved.

1. Introduction

The chemistry of quinoline and its derivatives has attracted special interest due to their therapeutic properties. Quinoline sulphonamides have been used in the treatment of cancer, tuberculosis, diabetes, malaria, and convulsion [1,2]. Apart from the magnetic and photophysical properties, the bioactivities of lanthanides such as antimicrobial, antitumor, antiviral, anticoagulant action, enhancing NK and macrophage cell activities, prevention from arteriosclerosis, etc., have been explored in recent decades [3–10]. In addition, Schiff bases are able to inhibit the growth of several animal tumors, and some metal chelates have shown good antitumor activities against animal tumors [11,12]. So, well-designed organic ligands enable a fine turning of special properties of the metal ions.

DNA is an important cellular receptor, many chemicals exert their antitumor effects by binding to DNA thereby changing the replication of DNA and inhibiting the growth of the tumor cells, which is the basis of designing new and more efficient antitumor drugs and their effectiveness depends on the mode and affinity of

the binding [13–15]. A number of metal chelates, as agents for mediation of strand scission of duplex DNA and as chemotherapeutic agents, have been used as probes of DNA structure in solution [16–18]. Albrecht and coworkers reported that both the crystal structures of [YLnO₃](DMF)₂Cl₂·2(DMF) and [LaL(NO₃)(MeOH)₂]₂(NO₃)₂ with nine-coordination have central planar four-membered (LaO)₂ and (YbO)₂ rings, respectively, where ligand L–H is 2-[(8-hydroxyquinolinyl)methylene]hydrazinecarboxamide and acts as a tetradentate ligand binding to yttrium(III) and lanthanum(III) [4]. Such structures may have strong affinities of binding to DNA through intercalations. In this paper, four Schiff-base ligands, which were structurally similar to the ligand L, were prepared from 8-hydroxyquinoline-2-carboxaldehyde with four aroylhydrazines to form their Dy(III) complexes and to investigate the DNA binding properties.

On the other hand, an excess of activated oxygen species in the forms of superoxide anion (O₂^{•-}) and hydroxyl radical (OH[•]), generated by normal metabolic processes, may cause various diseases such as carcinogenesis, drug-associated toxicity, inflammation, atherogenesis, and aging in aerobic organisms [19–21]. Although the naturally occurring antioxidants can scavenge free radicals in the body, they have been confined by their low effectiveness even though they are considered to be active in eliminating reactive oxygen and controlling toxic effects. The potential

* Corresponding author. Tel.: +86 931 8913515; fax: +86 931 8912582.

E-mail address: yangzy@lzu.edu.cn (Z.-y. Yang).

value of antioxidants has prompted investigators to search for the cooperative effects of metal complexes and natural compounds for improving antioxidant activity and cytotoxicity [22]. It has been recently demonstrated that some minor groove binders for DNA are effective inhibitors of the formation of a DNA/TBP complex or topoisomerases [23–25]. Adding a reactive entity endowed with oxidative properties should improve the efficiency of inhibitors. The antioxidation properties of the ligands and Dy(III) complexes were investigated in this paper. Furthermore, the substituent effects of these compounds on antioxidation and DNA binding properties were investigated further.

2. Chemistry

Four Schiff-base ligands, 8-hydroxyquinoline-2-carboxaldehyde-(benzoyl)hydrazine (**1a**, H_2L^1), 8-hydroxyquinoline-2-carboxaldehyde-(2'-hydroxybenzoyl)hydrazine (**1b**, H_2L^2), 8-hydroxyquinoline-2-carboxaldehyde-(4'-hydroxybenzoyl)hydrazine (**1c**, H_2L^3) and 8-hydroxyquinoline-2-carboxaldehyde-(isonicotinyl)hydrazine (**1d**, H_2L^4) were prepared from equimolar amounts of 8-hydroxyquinoline-2-carboxaldehyde and benzoylhydrazine, 2-hydroxybenzoylhydrazine, 4-hydroxybenzoylhydrazine, and isonicotinylhydrazine, respectively, whose structures were determined by IR spectroscopy, 1H NMR and ESI-MS. The synthetic routes for ligands are presented in Scheme 1. Then, their Dy(III) complexes (**2a–d**) were easily prepared from these ligands and equimolar amounts of $Dy(NO_3)_3 \cdot 6H_2O$, respectively.

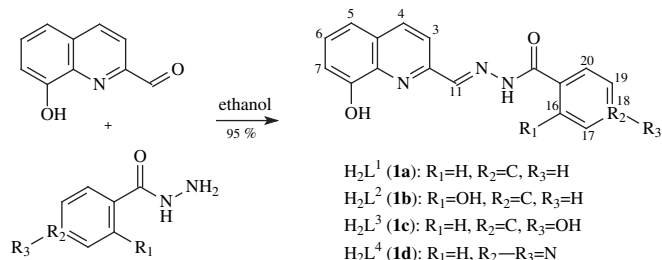
3. Results and discussion

3.1. Crystal structure analyses of the Dy(III) complexes

The orange transparent, X-ray quality crystals of complex **2a** and **2b** were obtained by vapor diffusion of diethyl ether into DMF solution of the powder complex at room temperature for 2 weeks, respectively. Crystal data and structure refinements for the X-ray structural analyses are presented in Table 1. Selected bond lengths and angles of the metal complexes are presented in Tables S1 and S2 (see Supplementary data Tables S1–S2).

3.1.1. The crystal structure of complex $[DyL^1(NO_3)(DMF)_2]_2$

The ORTEP illustration (30% probability ellipsoids) of complex **2a** in Fig. 1A shows that the complex composition is of $[DyL^1(-NO_3)(DMF)_2]_2$. Ligand **1a** acts as a dibasic tetradentate ligand, binding to Dy(III) through the phenolate oxygen atom, nitrogen atom of quinolinato unit and the C=N group, $^-O-C=N^-$ group (enolized and deprotonated from $O=C-NH^-$) of the benzoylhydrazine side chain. In addition, one DMF molecule is binding orthogonally to the ligand-plane from one side to the metal ion, while another DMF and nitrate (bidentate) are binding from the other. The center of symmetry according to the crystallographic coordinate is at 1/2, 0, 1/2. It is located in the middle of the four-



Scheme 1. The synthetic routes for ligands (**1a–d**).

membered $(DyO)_2$ ring formed by the two Dy atoms and the phenolic oxygen atoms. Dimerization of this monomeric unit occurs through the phenolate oxygen atoms leading to a central four-membered $(DyO)_2$ -ring with a Dy...Dy separation of 4.027 Å. At the dimerization site, a “set off” of the two “ DyL^1 -planes” by 1.637 Å takes place. This crystal structure of binuclear $[DyL^1(-NO_3)(DMF)_2]_2$ complex with a 1:1 metal-to-ligand stoichiometry and nine-coordination is similar to that of $[Yl(NO_3)(DMF)_2]_2Cl_2 \cdot 2(DMF)$ or $[LaL(NO_3)(MeOH)_2]_2(NO_3)_2$, where ligand L–H is 2-[(8-hydroxyquinolinyl)methylene]hydrazinecarboxamide and acts as a monad tetradentate ligand binding to yttrium(III) or lanthanum(III) through the phenolate oxygen atom, nitrogen atom of quinolinato unit and the C=N group, C=O group of the semicarbazone side chain [4]. However, there are two marked differences between them. One is that the “set off” of the two “ DyL^1 -planes” by 1.637 Å takes place while the “set off” of the two “Yl-planes” and “LaL-planes” by approximately 2 Å takes place. Another is that $O=C-NH^-$ group of the benzoylhydrazine side chain has enolized and deprotonated into $^-O-C=N^-$ group after the formation of $[DyL^1(NO_3)(DMF)_2]_2$ complex, where the C–O[−] single bond length is 1.294(4) Å and the N=C double bond length is 1.334(4) Å. Whereas the $O=C-NH^-$ group of the semicarbazone side chains has not enolized in $[Yl(NO_3)(DMF)_2]_2Cl_2 \cdot 2(DMF)$ or $[LaL(NO_3)(MeOH)_2]_2(NO_3)_2$ complex. The difference in the deprotonation and enolization may well be due to the fact that triethylamine was added into the reaction mixtures to deprotonate the phenolic hydroxyl substituent of 8-hydroxyquinolinato unit during the formation of the Dy(III) complex. It is the enolization and deprotonation of $O=C-NH^-$ group changing into $^-O-C=N^-$ that $[DyL^1(NO_3)(DMF)_2]_2$ is of neutral charge and non-electrolyte, but both of $[Yl(NO_3)(DMF)_2]_2Cl_2 \cdot 2(DMF)$ and $[LaL(NO_3)(MeOH)_2]_2(NO_3)_2$ are electrolytes. The enolization and deprotonation will afford an efficient route for investigators to design favorable molecules well.

3.1.2. The crystal structure of complex $[DyL^2(NO_3)(DMF)_2]_2$

The ORTEP illustration (30% probability ellipsoids) of complex **2b** in Fig. 1B shows that the complex composition is of $[DyL^2(-NO_3)(DMF)_2]_2$. The crystal of a binuclear $[DyL^2(NO_3)(DMF)_2]_2$ complex with a 1:1 metal-to-ligand stoichiometry and nine-coordination is much similar to that of $[DyL^1(NO_3)(DMF)_2]_2$. Both the complexes are almost isostructural. The center of symmetry is at 1, 1, and 0. It is located in the middle of the four-membered $(DyO)_2$ ring. Dimerization of this monomeric unit also occurs through the phenolate oxygen atoms leading to a central four-membered $(DyO)_2$ -ring with a Dy...Dy separation of 4.005 Å. At the dimerization site, a “set off” of the two “ DyL^2 -planes” by 1.640 Å takes place. The $O=C-NH^-$ group of the 2-hydroxybenzoylhydrazine side chain has also enolized and deprotonated into $^-O-C=N^-$ after the formation of $[DyL^2(NO_3)(DMF)_2]_2$ complex, where the ^-O-C and $N=C$ bond lengths are 1.273(3) and 1.327(3) Å, respectively. On the other hand, the 2-hydroxyl substituent linking with benzoylhydrazine has not take part in binding to Dy(III), largely due to the steric effect and long distance (5.217 Å) between the 2-hydroxyl substituent and Dy(III), but it may form an intramolecular hydrogen bond, a stabilizing six-membered ring, with adjacent nitrogen atom (1.843 Å) of the same side chain.

3.2. Structure analyses of the powder metal complexes

3.2.1. Elemental analysis and molar conductance

All the Dy(III) complexes are of orange powders, stable in air, and soluble in DMF and DMSO, but slightly soluble in methanol, ethanol, acetonitrile, ethyl acetate and acetone, THF and $CHCl_3$. The melting points of all the Dy(III) complexes exceed 300 °C.

Table 1
Crystal data and structure refinement of metal complexes.

Complex	$[\text{DyL}^1(\text{NO}_3)(\text{DMF})_2]_2$	$[\text{DyL}^2(\text{NO}_3)(\text{DMF})_2]_2$
Empirical formula	$\text{C}_{46}\text{H}_{50}\text{N}_{12}\text{O}_{14}\text{Dy}_2$	$\text{C}_{46}\text{H}_{50}\text{N}_{12}\text{O}_{16}\text{Dy}_2$
Formula weight	1319.98	1351.98
Crystal system	Monoclinic	Monoclinic
Space group	$P2_1/c$	$P2_1/c$
Unit cell dimensions	$a = 11.444(3) \text{ \AA}$, $\alpha = 90.00^\circ$ $b = 18.796(5) \text{ \AA}$, $\beta = 92.316(4)^\circ$ $c = 12.377(3) \text{ \AA}$, $\gamma = 90.00^\circ$	$a = 11.6129(6) \text{ \AA}$, $\alpha = 90.00^\circ$ $b = 18.0596(10) \text{ \AA}$, $\beta = 95.2960(10)^\circ$ $c = 12.7482(7) \text{ \AA}$, $\gamma = 90.00^\circ$
T	273(2) K	273(2) K
Volume	$2660.2(12) \text{ \AA}^3$	$2662.2(2) \text{ \AA}^3$
Z	2	2
Density (calculated)	1.648 mg/m^3	1.687 mg/m^3
Absorption coefficient	2.861 mm^{-1}	2.863 mm^{-1}
$F(000)$	1308	1340
Crystal size	$0.22 \times 0.20 \times 0.18 \text{ mm}^3$	$0.18 \times 0.15 \times 0.13 \text{ mm}^3$
Crystal description	Orange block	Orange block
θ Range for data collection	$1.78\text{--}26.49^\circ$	$1.76\text{--}28.35^\circ$
Index ranges	$-14 \leq h \leq 14$, $-23 \leq k \leq 18$, $-15 \leq l \leq 15$	$-15 \leq h \leq 14$, $-20 \leq k \leq 24$, $-15 \leq l \leq 14$
Reflections collected	14,615	15,968
Independent reflections	5488 ($R_{\text{int}} = 0.0281$)	6399 ($R_{\text{int}} = 0.0195$)
Absorption correction	Semi-empirical from equivalents	Semi-empirical from equivalents
Max. and min. transmission	0.597 and 0.539	0.688 and 0.601
Refinement method	Full-matrix least-squares on F^2	Full-matrix least-squares on F^2
Data/restraints/parameters	5488/0/338	6399/0/348
Goodness-of-fit on F^2	1.010	1.124
Final R indices [$I > 2\sigma(I)$]	$R_1 = 0.0234$, $wR_2 = 0.0462$	$R_1 = 0.0229$, $wR_2 = 0.0498$
R indices (all data)	$R_1 = 0.0392$, $wR_2 = 0.0504$	$R_1 = 0.0363$, $wR_2 = 0.0536$
Largest diff. peak and hole	0.601 and -0.379 e\AA^{-3}	0.600 and -0.522 e\AA^{-3}

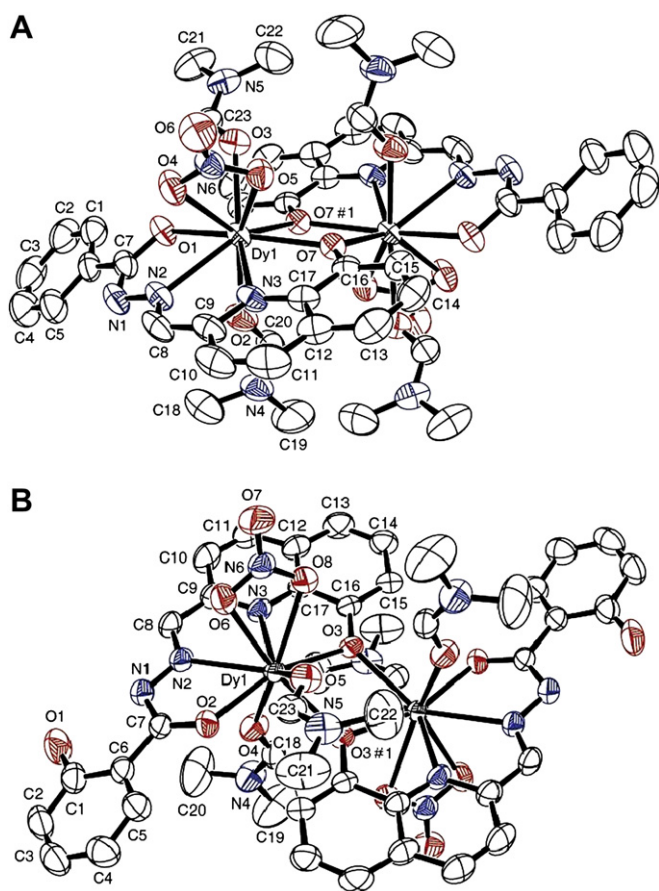


Fig. 1. The ORTEP illustration (30% probability ellipsoids) of $[\text{DyL}^1(\text{NO}_3)(\text{DMF})_2]_2$ (A) and $[\text{DyL}^2(\text{NO}_3)(\text{DMF})_2]_2$ (B) complexes.

Elemental analyses indicate that all the Dy(III) complexes are of 1:1 metal-to-ligand (stoichiometry) complexes, and the data of molar conductance of the Dy(III) complexes in DMF solutions indicate that all of them act as non-electrolytes [26].

3.2.2. Infrared spectrum study

The characteristic IR spectrum bands ($\nu_{\text{max}}/\text{cm}^{-1}$) of all the ligands showed $3576\text{--}3320_{\text{vs}}$ assigned to $\nu(\text{NH})$; $1682\text{--}1643_{\text{s}}$ assigned to $\nu(\text{CO})$ of the carbonyl groups of aroylhydrazine side chains and $1632\text{--}1602$ assigned to $\nu(\text{CN})$ of azomethines, whereas 1706_{s} assigned to $\nu(\text{CO})$ of the formyl disappeared. Moreover, $3318\text{--}3139_{\text{br}}$ and $1288\text{--}1267_{\text{s}}$ should be assigned to $\nu(\text{OH})$ and $\nu(\text{C}\text{--}\text{OH})$ of the phenolic hydroxyl substituents, respectively, and $1581\text{--}1532$ should be assigned to $\nu(\text{CN})$ of pyridines.

Carefully compared with the characteristic IR bands of ligands (data are listed in Table S3), it comes to the conclusion that: (1) $3406\text{--}3399_{\text{br}}$, $936\text{--}922_{\text{w}}$ and $642\text{--}612_{\text{w}}$ can be assigned to $\nu(\text{OH})$ of H_2O , $\rho_{\text{r}}(\text{H}_2\text{O})$ and $\rho_{\text{w}}(\text{H}_2\text{O})$, respectively, indicating that there are coordinated water molecules participating in the Dy(III) complexes [27,28]. (2) $1104\text{--}1102$ can be assigned to $\nu(\text{C}\text{--}\text{OM})$, indicating that the binding of metal ion to every ligand through an O–M linkage takes place [29]. (3) The new bands of 3216_{s} and 1256_{s} can be, respectively, assigned to $\nu(\text{OH})$ and $\nu(\text{C}\text{--}\text{OH})$ of the free phenolic hydroxyl substituent of 2-hydroxybenzoylhydrazine side chain of **2b** complex, and the new bands of 3193_{s} and 1289_{s} also can be, respectively, assigned to $\nu(\text{OH})$ and $\nu(\text{C}\text{--}\text{OH})$ of the phenolic hydroxyl substituent of 4-hydroxybenzoylhydrazine side chain of **2c** complex. (4) $1682\text{--}1643_{\text{s}}$ assigned to $\nu(\text{CO})$ and $3576\text{--}3320_{\text{vs}}$ assigned to $\nu(\text{NH})$ of aroylhydrazine side chains of ligands have disappeared, indicating that they participate in the Dy(III) complexes with the groups of $\text{O}=\text{C}\text{--}\text{NH}\text{--}$ of aroylhydrazine side chains enolized and deprotonated into $^-\text{O}=\text{C}=\text{N}\text{--}$ as proved by the above crystal structural analyses. (5) $1634\text{--}1598$ assigned to $\nu(\text{CN})$ of azomethines of the Dy(III) complexes has shifted by $34\text{--}38 \text{ cm}^{-1}$ in comparison with bands of ligands, indicating that the nitrogen atoms of azomethines participate in the complexes. (6) $1565\text{--}1548$ assigned to $\nu(\text{CN})$ of pyridines of the Dy(III) complexes has shifted

by 31–36 cm^{-1} in comparison with bands of ligands, indicating that the nitrogen atoms of pyridines also participate in the complexes. However, the new band of 1592 can be assigned to $\nu(\text{CN})$ of free pyridine of isonicotinylhydrazine side chain of **2d** complex. (7) 585–563 $_{\text{w}}$ assigned to $\nu(\text{MO})$ and 492–489 $_{\text{w}}$ assigned to $\nu(\text{MN})$ of the Dy(III) complexes further indicate that oxygen atoms and nitrogen atoms participate in Dy(III) complexes. (8) All the Dy(III) complexes show 1494–1491 (ν_1), 1336–1309 (ν_4), 1070–1058 (ν_2), 843–839 (ν_3), 761–740 (ν_5), and $\Delta\nu(\nu_1-\nu_4) = 184\text{--}158\text{ cm}^{-1}$, indicating that nitrate ions bidentately participate in the Dy(III) complexes [30].

Additionally, the ESI-MS data show that the m/z ($[\text{M} + \text{H}]^+$, DMF solution) are 1321.2, 1353.2, 1353.2 and 1323.2 for **2a**, **2b**, **2c** and **2d** complexes, respectively, indicating that the four coordinated water molecules for every powder Dy(III) complex can be replaced by four DMF molecules when dissolved in DMF solution. However, the results of elemental analyses, molar conductance, IR and ESI-MS data indicate that all the powder metal complexes are structurally similar to each other and their compositions are of $[\text{DyL}^{1-4}(\text{NO}_3)(\text{H}_2\text{O})_2]_2$.

3.3. DNA binding properties

3.3.1. Viscosity titration measurements

Viscosity measurements are very sensitive to changes in the length of DNA, as viscosity is proportional to L^3 for rod-like DNA of length L . Viscosity titration measurements were carried out to clarify the interaction modes between the investigated compounds and CT-DNA. Intercalation involves the insertion of a planar molecule between DNA base pairs, which results in a decrease in the DNA helical twist and lengthening of the DNA, therefore intercalators cause the unwinding and lengthening of DNA helix as base pairs become separated to accommodate the binding compound [31,32]. Whereas, agents bound to DNA through groove binding do not alter the relative viscosity of DNA, and agents electrostatically bound to DNA will bend or kink the DNA helix, reducing its effective length and its viscosity, concomitantly [33,34]. The effects of ligands and Dy(III) complexes on the viscosities of CT-DNA are shown in Fig. 2. With the ratios of the investigated compounds to DNA increase, the relative viscosities of DNA increase steadily, indicating that there exist intercalations between all the ligands and Dy(III) complexes with DNA helix. In addition, the relative viscosities of DNA increase with the order of **1a** > **1b** > **1c** > **1d** for ligands, the order of **2a** > **2b** > **2c** > **2d** for Dy(III) complexes, and the orders of **2a** > **1a**, **2b** > **1b**, **2c** > **1c** and **2d** > **1d**. These orders suggest the extents of the unwinding and lengthening of DNA helix by compounds and the affinities of compounds binding to DNA, which may be due to the key roles of substituent effects and the larger coplanar structures of Dy(III) complexes than those of ligands. Intercalation has been traditionally associated with molecules containing fused bi/tricyclic ring structures [35], so it is logical that all the large coplanar Dy(III) complexes containing fused multiple cyclic ring structures and all the ligands containing fused bicyclic ring structures can bind to DNA through intercalations.

3.3.2. Ultraviolet–visible (UV–Vis) spectroscopy study

The UV–Vis absorption spectra of the investigated compounds in the absence and in the presence of the CT-DNA were obtained in DMF:Tris–HCl buffer (5 mmol, pH 7.20) containing 50 mmol NaCl at 1:100 solutions, respectively (data are listed in Table S4). The UV–Vis spectra of ligands have two types of absorption bands at λ_{max} in the regions of 290–300 nm ($\epsilon = 2.86\text{--}3.55 \times 10^4\text{ dm}^3\text{ mol}^{-1}\text{ cm}^{-1}$) and 323–329 nm ($\epsilon = 1.78\text{--}2.36 \times 10^4\text{ dm}^3\text{ mol}^{-1}\text{ cm}^{-1}$), which can be assigned to $\pi\text{--}\pi^*$ transitions within the organic molecules, and $\pi\text{--}\pi^*$ of the C=N and C=O groups, respectively. While the UV–Vis

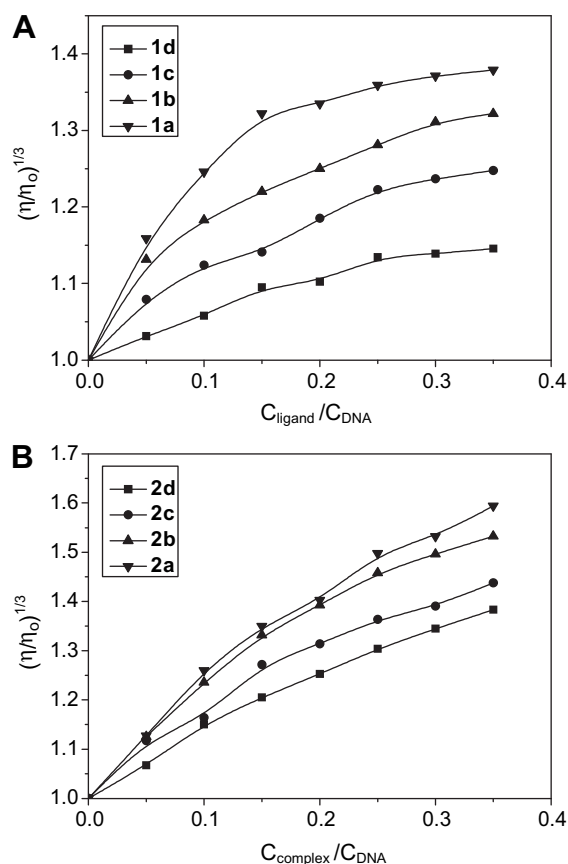


Fig. 2. Effects of increasing amounts of the investigated compounds on the relative viscosity of CT-DNA in 5 mmol Tris–HCl buffer solution (pH 7.20) containing 50 mmol NaCl at $25.00 \pm 0.01\text{ }^\circ\text{C}$. Plots of (A) and (B) represent the ligands–CT-DNA and Dy(III) complexes–CT-DNA systems, respectively. The concentration of CT-DNA was 50 μM (bps).

spectra of Dy(III) complexes have two types of absorption bands at λ_{max} in the regions of 326–332 nm ($\epsilon = 2.94\text{--}4.49 \times 10^4\text{ dm}^3\text{ mol}^{-1}\text{ cm}^{-1}$) and 372–379 nm ($\epsilon = 2.99\text{--}3.73 \times 10^4\text{ dm}^3\text{ mol}^{-1}\text{ cm}^{-1}$), which can be, respectively, assigned to $\pi\text{--}\pi^*$ transitions of the larger conjugated organic molecules and $\pi\text{--}\pi^*$ of the C=N–N=C groups coupled with charge transfers from ligands to metal ions ($\text{L} \rightarrow \text{Dy}^{3+}$) [27,28]. The band shifts of λ_{max} and the changes of ϵ for complexes in comparison with ligands indicate the formations of the Dy(III) complexes.

Upon successive additions of CT-DNA, the UV–Vis absorption bands of ligands **1a**, **1b**, **1c** and **1d** show a progressive hypochromism of 34.3% at 295 nm, 30.1% at 294 nm, 22.5% at 300 nm and 8.4% at 290 nm by approximately saturated titration end points at $C_{\text{DNA}}:C_{\text{ligand}} = 1.4\text{--}2.2:1$, respectively, with a 1, 3, 1 and 0 nm red shifts of absorption bands in the region of 290–300 nm. Ligands **1a**, **1b**, **1c** and **1d** show another progressive hypochromism of 11.1% at 323 nm, 18.1% at 329 nm, 4.8% at 326 nm and 1.0% at 325 nm, respectively, with a 1, 3, 1 and 0 nm blue shifts in the region of 323–329 nm. Similarly, upon successive additions of CT-DNA, the UV–Vis absorption bands of metal complexes **2a**, **2b** and **2c** show a progressive hypochromism of 40.6% at 326 nm, 23.3% at 327 nm and 22.2% at 332 nm by approximately saturated titration end points at $C_{\text{DNA}}:C_{\text{complex}} = 1.0\text{--}1.4:1$, respectively, but all of them have no shift of absorption bands. Complexes **2a**, **2b** and **2c** show another progressive hypochromism of 38.5% at 373 nm with 1 nm blue shift, 23.8% at 377 nm with 5 nm red shift and 20.1% at 379 nm with no band shift, respectively. Complex **2d** shows two types of

slightly unsteady hypochromisms of 0.45% at 327 nm with 1 nm blue shift and 0.72% at 372 nm with 1 nm red shift by an approximately saturated titration end point at $C_{\text{DNA}}:C_{\text{complex}} = 1.4:1$. In addition, isosbestic points at 342–357 nm for ligands and at 404–423 nm for Dy(III) complexes are observed, indicating that the reaction between every investigated compound and DNA takes places by an equilibrium.

Absorption titration can monitor the interaction of a compound with DNA. The obvious hypochromism and red shift are usually characterized by the noncovalently intercalative binding of compound to DNA helix, due to the strong stacking interaction between the aromatic chromophore of the compound and base pairs of DNA [36,37]. However, the intercalation between a compound and DNA helix cannot be excluded only by no or small red shift of UV-Vis absorption bands. In fact, some groove binders of Hoechst 33258 family can also present red shifts or even blue shifts of absorption bands when they bind to DNA helix by groove binding modes, especially for multiple binders [38,39]. After all, hydrodynamic measurements that are sensitive to length change of DNA (*i.e.*, viscosity and sedimentation) are regarded as the least ambiguous and the most critical criterions for binding modes in solution in the absence of crystallographic structural data [40,41].

On the other hand, the magnitude of hypochromism is parallel to the intercalative strength and the affinity of a compound binding to DNA [42]. The appreciable hypochromisms of ligands and Dy(III) complexes intercalating to DNA present the order of $1\mathbf{a} > 1\mathbf{b} > 1\mathbf{c} > 1\mathbf{d}$ and the order of $2\mathbf{a} > 2\mathbf{b} > 2\mathbf{c} > 2\mathbf{d}$, which are in good agreement with the orders of viscosity titration results. Here, the substituent effects may play key roles in the interactions. Besides the same structural units of these Dy(III) complexes, as for complex $2\mathbf{a}$, the phenyl substituent may be more accessible to DNA helix and much favorable of forming π - π stacking interaction between the aromatic chromophore of the complex and the base pairs of DNA than 2-hydroxyphenyl and 4-hydroxyphenyl substituents of $2\mathbf{b}$ and $2\mathbf{c}$ complexes. For complex $2\mathbf{b}$, 2-hydroxy locating in benzoylhydrazine side chain may form an intramolecular hydrogen bond, a stabilizing six-membered ring that is coplanar to one of DyL^2 -planes, with adjacent nitrogen atom of the same side chain, which will induce smaller steric hindrances than exposed 4-hydroxy locating in benzoylhydrazine side chain for complex $2\mathbf{c}$. As for complex $2\mathbf{d}$, *N* atom of aromatic sextet of the pyridine ring of isonicotinylhydrazine side chain has an exposed and non-hybridized *p* orbital containing long pair electrons, which may result in a stronger electronic repulsion and hinder the π - π stacking interaction. Moreover, the aggregation of self-stacked molecules of $2\mathbf{d}$ may occur in the absence of DNA, even in an excess of conjugate versus DNA bps, which induces the possibility of an association/dissociation equilibrium in the reaction solution, concomitantly, induces a slightly unsteady and small hypochromism of UV-Vis absorption [39].

3.3.3. EtBr-DNA quenching assay

The fluorescence emission intensity of EtBr-DNA system decreased dramatically upon the increasing amounts of every ligand and Dy(III) complex. Stern-Volmer equation was used to determine the fluorescent quenching mechanism [31]. Plots of F_0/F versus $[Q]$ are shown in Fig. 3 and the quenching data collected and calculated from the good linear relationship when $P < 0.05$ are listed in Table 2. As shown, the data of K_{SV} are 1.405 – $3.016 \times 10^4 \text{ M}^{-1}$ for ligands and 3.547 – $13.06 \times 10^4 \text{ M}^{-1}$ for Dy(III) complexes, accordingly, the data of K_{q} calculated are 0.7806 – $1.676 \times 10^{13} \text{ M}^{-1} \text{ s}^{-1}$ for ligands and 1.971 – $7.256 \times 10^{13} \text{ M}^{-1} \text{ s}^{-1}$ for Dy(III) complexes, respectively, when the value of τ_0 is taken as $1.8 \times 10^{-9} \text{ s}$ [31]. All of the current values of K_{q} for ligands and Dy(III) complexes are much greater than that of $K_{\text{q}(\text{max})}$

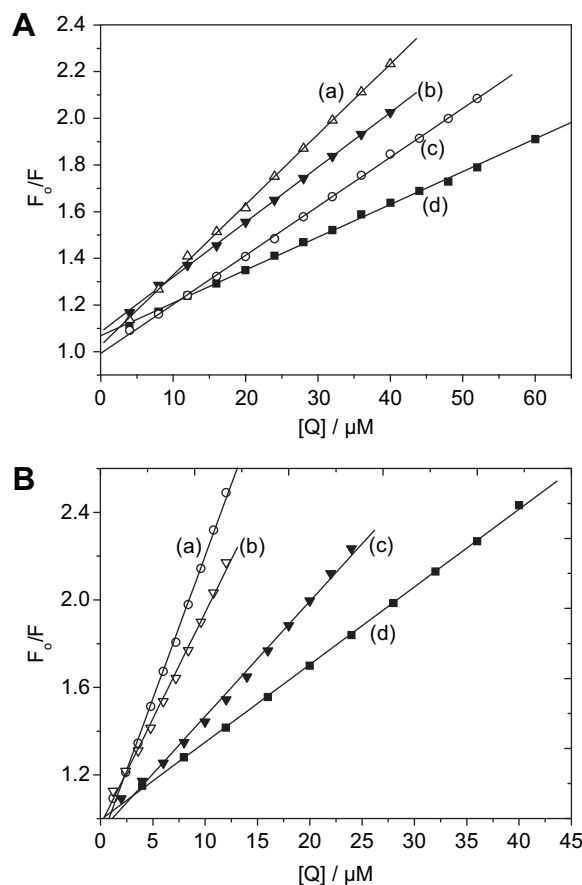


Fig. 3. Stern-Volmer plots of F_0/F versus $[Q]$ for ligands (A) and Dy(III) complexes (B). Tests were performed in the conditions of 5 mmol Tris-HCl buffer containing 50 mmol NaCl at 298 K. $C_{\text{DNA}} = 4 \mu\text{M}$ (nucleotides), $C_{\text{EtBr}} = 0.32 \mu\text{M}$; $\lambda_{\text{ex}} = 525 \text{ nm}$, $\lambda_{\text{em}} = 587 \text{ nm}$. Lines of (a), (b), (c) and (d) in plot (A) for ligand $1\mathbf{c}$, $1\mathbf{b}$, $1\mathbf{a}$ and $1\mathbf{d}$, respectively, while lines of (a), (b), (c) and (d) in plot (B) for complex $2\mathbf{c}$, $2\mathbf{b}$, $2\mathbf{a}$ and $2\mathbf{d}$, respectively.

($2.0 \times 10^{10} \text{ M}^{-1} \text{ s}^{-1}$), the maximum quenching rate constant of bimolecular diffusion collision, which are indicative of static types of quenching mechanisms arisen from the formations of dark complexes between the fluorophores and quenching agents [43,44]. The loss of fluorescence intensity at the maximum wavelength indicates the displacement of EtBr from EtBr-DNA complex by a compound and the intercalative binding between the compound with DNA [34]. The EtBr-DNA quenching results indicate that most of the EtBr molecules have been displaced from EtBr-DNA complex by every quencher at the approximately saturated end point. Thus, it is reasonable that there exist intercalations between DNA and these investigated compounds.

Moreover, the Stern-Volmer dynamic quenching constants can also be interpreted as binding affinities of the complexation reactions [45,46]. The data of K_{SV} present the order of $1\mathbf{c} > 1\mathbf{b} > 1\mathbf{a} > 1\mathbf{d}$ for ligands, the order of $2\mathbf{c} > 2\mathbf{b} > 2\mathbf{a} > 2\mathbf{d}$ for complexes, and the orders of $2\mathbf{a} > 1\mathbf{a}$, $2\mathbf{b} > 1\mathbf{b}$, $2\mathbf{c} > 1\mathbf{c}$, $2\mathbf{d} > 1\mathbf{d}$, which indicate the abilities of displacement of EtBr from EtBr-DNA systems by compounds and the binding affinities between compounds and DNA. However, the orders are not slightly in good agreement with the viscosity titration and UV-Vis spectroscopy study results. Here, the phenolic hydroxy groups that can bind to nucleotides or/and the sugar-phosphate backbone of DNA through hydrogen bonds may play certain roles in the EtBr-DNA quenching tests. However, the other weak interactions such as hydrophobic force, Van der Waals force and electrostatic force (pH at 7.20) may not be excluded. In other words, the interaction mechanism is not only

Table 2
Parameters of K_b , K_{SV} , K_q , CF_{50} , IC_{50} (OH^\cdot and $O_2^{\cdot-}$) for ligands and the Dy(III) complexes.

Compounds	$K_b \times 10^6 M^{-1}$	$1/n^a$	$K_{SV} \times 10^4 M^{-1} (R)$	$K_q \times 10^{13} M^{-1} s^{-1}$	$CF_{50}^b \times 10^{-5} M$ ($C_{\text{compound}}/C_{\text{DNA, nucleotides}}$)	IC_{50}^c (μM) for OH^\cdot (R)	IC_{50}^c (μM) for $O_2^{\cdot-}$ (R)
1a	0.2148 \pm 0.0205	0.081	2.086 \pm 0.014 (0.9997)	1.159	4.818 (12.05)	14.66 \pm 0.495 (0.9937)	6.831 \pm 0.219 (0.9954)
1b	0.9295 \pm 0.1315	0.28	2.352 \pm 0.018 (0.9998)	1.307	3.895 (9.738)	7.716 \pm 0.230 (0.9940)	4.308 \pm 0.174 (0.9892)
1c	0.7599 \pm 0.0867	0.066	3.016 \pm 0.027 (0.9997)	1.676	3.229 (8.073)	11.38 \pm 0.441 (0.9902)	4.096 \pm 0.112 (0.9955)
1d	0.1329 \pm 0.0180	0.092	1.405 \pm 0.013 (0.9995)	0.7806	6.630 (16.58)	76.10 \pm 0.372 (0.9909)	5.131 \pm 0.258 (0.9838)
2a	5.687 \pm 1.084	0.14	4.588 \pm 0.083 (0.9990)	2.549	2.200 (5.500)	13.80 \pm 0.303 (0.9914)	7.971 \pm 0.517 (0.9768)
2b	13.41 \pm 4.760	0.15	9.697 \pm 0.232 (0.9977)	5.387	1.061 (2.653)	5.815 \pm 0.133 (0.9925)	29.20 \pm 1.54 (0.9930)
2c	26.94 \pm 3.540	0.18	13.06 \pm 0.211 (0.9990)	7.256	0.8465 (2.116)	4.687 \pm 0.086 (0.9948)	16.17 \pm 1.37 (0.9663)
2d	0.5783 \pm 0.0959	0.35	3.547 \pm 0.021 (0.9957)	1.971	2.832 (7.080)	18.75 \pm 0.423 (0.9795)	5.646 \pm 0.437 (0.9525)

^a The data of $1/n$ represent moles of compound/mol of base pair of DNA.

^b CF_{50} represents the molar concentration of the tested compound that causes a 50% loss in the fluorescence intensity of EtBr–DNA system.

^c IC_{50} value was calculated from regression line of the log of the tested compound concentration versus the scavenging effect (%) of the compound. R represents the linear correlation coefficient.

determined by complex formation but also by certain weak interactions [47].

More importantly, DNA intercalators have been used extensively as antitumor, antineoplastic, antimalarial, antibiotic, and antifungal agents [31]. There is a criterion for screening out antitumor drugs from others by EtBr–DNA fluorescent tracer method, *i.e.*, a compound can be used as potential antitumor drug if it can cause a 50% loss of EtBr–DNA fluorescence intensity by fluorescent titrations before the molar concentration ratio of the compound to DNA (nucleotides) does not overrun 100:1 [48]. CF_{50} value is introduced to denote the molar concentration of a compound that causes a 50% loss in the fluorescence intensity of EtBr–DNA system. According to the data of CF_{50} and the molar ratios of compounds to DNA shown in Table 2, it is interesting that at CF_{50} , all the molar concentration ratios of the investigated compounds to DNA are largely under 100:1, indicating that all these ligands and Dy(III) complexes can be used as potential antitumor drugs and the antitumor activities of Dy(III) complexes are more excellent than those of ligands. However, their pharmacodynamical and pharmacological properties should be further studied *in vivo*.

3.3.4. Fluorescence spectroscopy study

When excited at $\lambda_{ex} = 321\text{--}325$ nm, ligands showed the fluorescence maximum wavelengths at $\lambda_{em} = 429\text{--}444$ nm, and excited at $\lambda_{ex} = 333\text{--}334$ nm the Dy(III) complexes showed the fluorescence maximum wavelengths at $\lambda_{em} = 426\text{--}433$ nm, respectively. Upon additions of DNA, the fluorescence emission intensity of every investigated compound grew steadily. Although the emission enhancement cannot be regarded as a rigid criterion for binding mode, it is related to the extent to which the compound gets into a hydrophobic environment inside DNA and avoids the effect of solvent water molecules. To compare quantitatively the affinities of these compounds bound to DNA, the intrinsic binding constants K_b can be obtained by the fluorescence titration methods and Scatchard equation [34,49]. Scatchard plot should be a straight line for a simple binding reaction [50]. Because of the significant neighbour exclusion property of DNA binding to intercalating agents, the Scatchard plot of r/C_f versus r usually presents a deviation from linearity [51]. As shown in Fig. S1, every plot of r/C_f versus r for ligands and Dy(III) complexes shows a deviation from linearity, so the binding constant was obtained by McGhee and von Hippel model [51,52]. The data of binding constants (K_b) and the moles of compound bound per mol of base pair of DNA ($1/n$) are shown in Table 2. It is clear that the data of binding constants (K_b) present the order of **1b** > **1c** > **1a** > **1d** for ligands, which is slightly different from the order of EtBr–DNA quenching result. But the data of binding constants (K_b) present the orders of **2a** > **1a**, **2b** > **1b**, **2c** > **1c**, **2d** > **1d**, and the order of **2c** > **2b** > **2a** > **2d** for complexes,

which are consistent with the orders of EtBr–DNA quenching results. Although it is a weaker binding for complex **2d** to DNA, they are stronger bindings for complexes **2c**, **2b** and **2a** to DNA in comparison with the classical intercalator (EtBr–DNA, $K_b = 3.0 \times 10^6 M^{-1}$ in 5 mmol Tris–HCl/50 mmol NaCl buffer, pH = 7.2), indicating that these three Dy(III) complexes can bind to DNA effectively [53,54].

3.4. Antioxidation properties

3.4.1. Hydroxyl radical scavenging activity

Fig. 4A and B shows the plots of hydroxyl radical scavenging effect (%) for ligands and Dy(III) complexes, respectively, which are concentration-dependant. As shown in Table 2, the values of IC_{50} of ligands for OH^\cdot are $7.716 \pm 0.230\text{--}76.10 \pm 0.372 \mu M$ with the order of **1b** < **1c** < **1a** < **1d**, while the values of IC_{50} of Dy(III) complexes for OH^\cdot are $5.815 \pm 0.133\text{--}18.75 \pm 0.423 \mu M$ with the order of **2c** < **2b** < **2a** < **2d**. These orders of IC_{50} are opposite to the abilities of scavenging effects for OH^\cdot . It is marked that the hydroxyl radical scavenging effects of Dy(III) complexes are much higher than those of their ligands, possibly in that the larger conjugated metal complexes can react with HO^\cdot to form larger stable macromolecular radicals than ligands [55]. Moreover, ligands **1b**, **1c** and their Dy(III) complexes show higher abilities of scavenging effects for OH^\cdot than other ligands and Dy(III) complexes, possibly due to the key roles of functional groups, $-OH$, which can react with HO^\cdot to form stable macromolecular radicals by the typical H-abstraction reaction [55]. Furthermore, for OH^\cdot , there are two types of antioxidation mechanisms, in which one presents suppression of the generation of OH^\cdot , and another presents scavenging of the OH^\cdot generated [55]. OH^\cdot production, detected by ethylene formation from methional, has been investigated in plasma, lymph and synovial fluid in the previous study [56]. In the presence of iron–EDTA as a catalyst, addition of either H_2O_2 or xanthine and xanthine oxidase give rise to OH^\cdot formation that in most cases is not superoxide-dependent. In the absence of iron–EDTA, the reaction is hardly detectable, the rate being less than 5% of that observed with $1 \mu M$ iron–EDTA added. In the present study, the chelation between phenolic hydroxyl group and carbonyl group of 2-hydroxybenzoylhydrazine side chain for ligand **1b** with free Fe^{2+} in iron–EDTA reaction system may make the concentration of free Fe^{2+} much lower so that the catalysis becomes very poor and the OH^\cdot formation has been suppressed, thus, the inhibitive effect of **1b** detected for OH^\cdot is higher than those of other ligands. However, after formation of Dy(III) complex, the chelation between **1b** and free Fe^{2+} may be destroyed with the formation of intramolecular hydrogen bonds for **2b**, so the hydroxyl radical scavenging effect (%) of **2b** is slightly lower than that of complex **2c**.

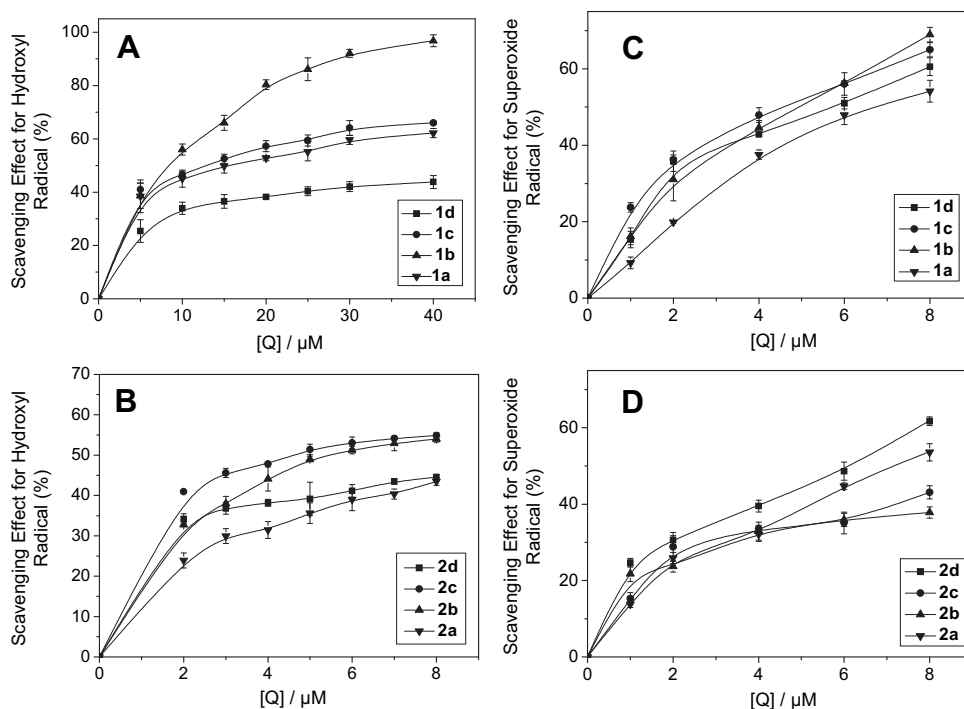


Fig. 4. Plots of antioxidation properties for ligands and Dy(III) complexes. (A) and (B) represent the hydroxyl radical scavenging effect (%) for ligands and Dy(III) complexes, respectively. (C) and (D) represent the superoxide radical scavenging effect (%) for ligands and Dy(III) complexes, respectively.

3.4.2. Superoxide radical scavenging activity

Fig. 4C and D shows the plots of superoxide radical scavenging effects (%) for ligands and Dy(III) complexes, respectively, which are also concentration-dependant, but both the plots slightly blend together. As shown in Table 2, the values of IC_{50} of ligands for $O_2^{\cdot -}$ are 4.096 ± 0.112 – $6.831 \pm 0.219 \mu\text{M}$ with no significant difference from each other, but the values of IC_{50} of Dy(III) complexes for $O_2^{\cdot -}$ are 5.646 ± 0.437 – $29.20 \pm 1.54 \mu\text{M}$ with a notably different order of $2d < 2a < 2c < 2b$. These results suggest that complex containing *N*-heteroaromatic substituent shows stronger scavenging effects for $O_2^{\cdot -}$, and that there are different mechanisms between scavenging and inhibiting OH^{\cdot} and $O_2^{\cdot -}$, which should be further studied.

It is reported that the value of IC_{50} of ascorbic acid (Vc), a standard agent for non-enzymatic reaction, for OH^{\cdot} is 1.537 mg cm^{-3} (8.727 mmol), and the scavenging effect of Vc for $O_2^{\cdot -}$ is only 25% at 1.75 mg cm^{-3} (9.94 mmol) *in vitro* [57]. It is pronounced that all the ligands and the Dy(III) complexes investigated here have much stronger scavenging abilities for OH^{\cdot} and $O_2^{\cdot -}$ than ascorbic acid (Vc). Endowed with antioxidative properties, these DNA binders may be effective inhibitors of the formation of a DNA/TBP complex topoisomerases [23–25].

4. Conclusion

The Dy(III) complexes are prepared from $\text{Dy}(\text{NO}_3)_3 \cdot 6\text{H}_2\text{O}$ and Schiff-base ligands derived from 8-hydroxyquinoline-2-carboxaldehyde with four aroylhydrazines, respectively. X-ray crystals and other structural analyses show that Dy(III) and every ligand can form a binuclear Dy(III) complex with a 1:1 metal-to-ligand stoichiometry and nine-coordination at the Dy(III) center. Every ligand acts as a dibasic tetradentate ligand, binding to Dy(III) through the phenolate oxygen atom, nitrogen atom of quinolinato unit and the $\text{C}=\text{N}$ group, $^-\text{O}-\text{C}=\text{N}-$ group (enolized and deprotonated from $\text{O}=\text{C}-\text{NH}-$ group) of the aroylhydrazine side chain. Dimerization of this monomeric unit occurs through the phenolate oxygen atoms

leading to a central four-membered $(\text{DyO})_2$ -ring. It is the key role of enolization and deprotonation that the dimeric centronucleus of every Dy(III) complex is of neutral charge, which will afford an efficient route for investigators to well design favorable molecules. In addition, all the ligands and Dy(III) complexes can bind to CT-DNA through intercalations with the binding constants at 10^5 – 10^7 M^{-1} , but Dy(III) complexes present stronger affinities to DNA than ligands. **2a**, **2b** and **2c** complexes can bind to DNA effectively. All the ligands and Dy(III) complexes can be used as potential anticancer drugs but the antitumor activities of Dy(III) complexes are more excellent than those of ligands. However, their pharmacodynamical and pharmacological properties should be further studied *in vivo*.

On the other hand, all the ligands and Dy(III) complexes have strong abilities of antioxidation but Dy(III) complexes show stronger scavenging effects for OH^{\cdot} than ligands. Dy(III) complexes or ligands containing active phenolic hydroxy groups present stronger abilities of scavenging effects for OH^{\cdot} than others, but complex containing *N*-heteroaromatic substituent shows stronger scavenging effects for $O_2^{\cdot -}$.

5. Experimental protocols

5.1. Materials

Calf thymus DNA (CT-DNA) and ethidium bromide (EtBr) were obtained from Sigma–Aldrich Biotech. Co., Ltd. 8-Hydroxyquinoline-2-carboxaldehyde was obtained from J&K Chemical Co., Ltd. All the stock solutions (1.0 mmol) of the investigated compounds were prepared by dissolving the powder materials into appropriate amounts of DMF solutions, respectively. Deionized double distilled water and analytical grade reagents were used throughout.

CT-DNA stock solution was prepared by dissolving the solid material in 5 mmol Tris–HCl buffer (pH 7.20) containing 50 mmol NaCl. Then, the solution was kept over 48 h at 4°C . The resulting somewhat viscous solution was clear and particle-free. The solution

of CT-DNA in Tris–HCl buffer gave a ratio of UV–Vis absorbance at 260–280 nm of about 1.8–1.9, indicating that the CT-DNA was sufficiently free of protein. The CT-DNA concentration in terms of base pair L^{-1} was determined spectrophotometrically by employing an extinction coefficient of $\epsilon = 13200 M^{-1} cm^{-1}$ (base pair) $^{-1}$ at 260 nm. The CT-DNA concentration in terms of nucleotide L^{-1} was also determined spectrophotometrically by employing an extinction coefficient of $6600 M^{-1} cm^{-1}$ (nucleotide) $^{-1}$ at 260 nm [58]. The stock solution was stored at $-20\text{ }^{\circ}C$ until it was used. Working standard solution of CT-DNA was obtained by appropriate dilution of the stock solution in 5 mmol Tris–HCl buffer (pH 7.20) containing 50 mmol NaCl. EtBr was dissolved in 5 mmol Tris–HCl buffer (pH 7.20) and its concentration was determined assuming a molar extinction coefficient of $5600 L mol^{-1} cm^{-1}$ at 480 nm [31].

5.2. Methods

The melting points of the compounds were determined on an XT4-100X microscopic melting point apparatus (Beijing, China). Elemental analyses of C, N and H were carried out on an Elemental Vario EL analyzer. The metal ion content was determined by complexometric titration with EDTA after destruction of the complex in the conventional manner. The IR spectra were recorded on a Nicolet Nexus 670 FT-IR spectrometer using KBr disc in the $4000\text{--}400 cm^{-1}$ region. 1H NMR spectra were recorded on a Bruker Avance DRX 200-MHz spectrometer with tetramethylsilane (TMS) as an internal standard. ESI-MS (ESI-Trap/Mass) spectra were recorded on a Bruker esquire6000 mass spectrophotometer.

Viscosity titration experiments were carried on an Ubbelodde viscometer in a thermostated water-bath maintained at $25.00 \pm 0.01\text{ }^{\circ}C$. Titrations were performed for an investigated compound that was introduced into DNA solution (50 μM , bps) present in the viscometer. Data were presented as $(\eta/\eta_0)^{1/3}$ versus the ratio of the compound to DNA, where η is the viscosity of DNA in the presence of the compound corrected from the solvent effect, and η_0 is the viscosity of DNA alone. Relative viscosities for DNA in either the presence or absence of compound were calculated from the following relation:

$$\eta = (t - t_0)/t_0 \quad (1)$$

where t is the observed flow time of the DNA containing solution, and t_0 is the flow time of buffer [31,33].

Ultraviolet–visible (UV–Vis) spectra were obtained using a PerkinElmer Lambda UV–Vis spectrophotometer.

Fluorescence spectra were recorded using RF-5301PC spectrofluorophotometer (Shimadzu, Japan) with a 1 cm quartz cell. Both the excitation and emission bandwidths were 10 nm. All the experiments were measured after 5 min at a constant room temperature, 298 K. The intrinsic binding constants K_b could be obtained by the fluorescence titration methods and Scatchard equation [49]:

$$r/C_f = nK_b - rK_b \quad (2)$$

where r is the moles of compound bound per mole nucleotides of DNA; C_f is the molar concentration of free compound; n is the number of binding sites or the maximum number of compound bound per nucleotide, and K_b is the association or binding constant. C_f and r could be calculated according to the following equations [34]:

$$C_f = C_t - C_b \quad (3)$$

$$C_b = C_t(F - F_0)/(F_{\max} - F_0) \quad (4)$$

$$r = C_b/C_{\text{DNA}} \quad (5)$$

where C_t is the total molar concentration of compound; C_b is the molar concentration of compound bound for DNA; F is the observed fluorescence emission intensity at a given DNA concentration C_{DNA} (nucleotides); F_0 is the fluorescence emission intensity in the absence of DNA; and F_{\max} is the maximum fluorescence emission intensity of the compound totally bound for DNA at a titration end point.

The binding constants were also obtained by McGhee and von Hippel model [51,52]:

$$\frac{r}{C_f} = K_b(1 - nr) \left[\frac{1 - nr}{1 - (n-1)r} \right]^{n-1} \quad (6)$$

where K_b is the intrinsic binding constant and n is the exclusion parameter in DNA base pairs. The experimental parameters K_b and n were adjusted to produce curves that gave, by inspection, the most satisfactory fits to the experimental data.

EtBr–DNA quenching assay was performed as reported in a literature with a slight amendment [59]. DNA (4.0 μM , nucleotides) solution was added incrementally to 0.32 μM EtBr solution, until the rise in the fluorescence ($\lambda_{\text{ex}} = 496\text{ nm}$, $\lambda_{\text{em}} = 596\text{ nm}$) attained a saturation. Then, small aliquots of concentrated compound solutions (1.0 mmol) were added till the drop in fluorescence intensity ($\lambda_{\text{ex}} = 525\text{ nm}$, $\lambda_{\text{em}} = 587\text{ nm}$) reached a constant value. The experiments were measured after 5 min at a constant room temperature, 298 K. Stern–Volmer equation was used to determine the fluorescent quenching mechanisms [31]:

$$F_0/F = 1 + K_q\tau_0[Q] = 1 + K_{SV}[Q] \quad (7)$$

where F_0 and F are the fluorescence intensities in the absence and in the presence of a compound at $[Q]$ concentration, respectively; K_{SV} is the Stern–Volmer dynamic quenching constant; K_q is the quenching rate constant of bimolecular diffusion collision; τ_0 is the lifetime of free EtBr.

The hydroxyl radicals in aqueous media were generated through the Fenton-type reaction [56,60]. The 5 cm^3 reaction mixtures contained 2.0 cm^3 of 100 mmol phosphate buffer (pH = 7.4), 1.0 cm^3 of 0.10 mmol aqueous safranin, 1 cm^3 of 1.0 mmol aqueous EDTA–Fe(II), 1 cm^3 of 3% aqueous H_2O_2 , and a series of quantitatively microadding solutions of the tested compound. The sample without the tested compound was used as the control. The reaction mixtures were incubated at $37\text{ }^{\circ}C$ for 60 min in a water-bath. Absorbance at 520 nm was measured and the solvent effect was corrected throughout. The scavenging effect for OH^{\cdot} was calculated from the following expression:

$$\text{Scavenging effect (\%)} = \frac{A_{\text{sample}} - A_{\text{blank}}}{A_{\text{control}} - A_{\text{blank}}} \times 100 \quad (8)$$

where A_{sample} is the absorbance of the sample in the presence of the tested compound, A_{blank} is the absorbance of the blank in the absence of the tested compound and A_{control} is the absorbance in the absence of the tested compound and EDTA–Fe(II) [34,61].

The superoxide radicals were produced by the MET–VitB₂–NBT system [34,61]. The solutions of MET (methionine), VitB₂ (vitamin B₂), and NBT (nitroblue tetrazolium) were prepared with deionized double distilled water at avoiding light, respectively. The 5 cm^3 reaction mixtures contained 2.5 cm^3 of 100 mmol phosphate buffer (pH 7.8), 1.0 cm^3 of 50 mmol MET, 1.0 cm^3 of 0.23 mmol NBT, 0.50 cm^3 of 33 μM VitB₂, and a series of quantitatively microadding solutions of the tested compound. After incubated at $30\text{ }^{\circ}C$ for 10 min in a water-bath and then illuminated with a fluorescent lamp (4000 lux), the absorbance of the sample was measured at

560 nm and the solvent effect was corrected throughout. The sample reaction mixtures without the tested compound were used as the control. The scavenging effect for $O_2^{\cdot-}$ was calculated from the following expression:

$$\text{Scavenging effect (\%)} = \frac{A_0 - A_i}{A_0} \times 100 \quad (9)$$

where A_i is the absorbance in the presence of the tested compound, A_0 is the absorbance in the absence of the tested compound.

The data for antioxidation presented as means \pm SD of three determinations and followed by Student's *t*-test. Differences were considered to be statistically significant if $P < 0.05$. IC_{50} value was introduced to denote the molar concentration of the tested compound which caused a 50% inhibitory or scavenging effect on hydroxyl radicals or superoxide radicals.

5.3. Preparation of ligands

5.3.1. 8-hydroxyquinoline-2-carboxaldehyde-(benzoyl)hydrazone (**1a**)

Ligand **1a** was prepared by refluxing and stirring a 10 cm^3 ethanol solution of 8-hydroxyquinoline-2-carboxaldehyde (0.519 g, 3 mmol) and a 10 cm^3 90% ethanol aqueous solution of benzoylhydrazine (0.408 g, 3 mmol) for 8 h. After cooling to room temperature, the precipitate was filtered, recrystallized from 80% methanol aqueous solution and dried in vacuum over 48 h to give a pale yellow powder. Yield: 74.7% (0.656 g); m.p. = 221 °C; ESI-MS m/z 292.1 $[M + H]^+$; 1H NMR (DMSO- d_6 , 200 MHz, TMS) δ : 8.637 (s, 1 H, 11-CH=N), 8.343 (d, $J = 8.8$ Hz, 1 H, 4-CH), 8.119 (d, $J = 8.8$ Hz, 1 H, 3-CH), 7.936 (d, $J = 6.4$ Hz, 2 H, 16,20-CH), 7.630–7.507 (m, 3 H, 17,18,19-CH), 7.467–7.387 (m, 2 H, 5,6-CH), 7.131 (d, 1 H, $J = 5.0$ Hz, 7-CH); IR (KBr): (cm^{-1}): 3359, 3318, 1682, 1602, 1546, 1267; UV-Vis (DMF/H₂O): λ_{max} (ϵ) = 295 (35,500), 323 nm (21100 $M^{-1} cm^{-1}$).

5.3.2. 8-hydroxyquinoline-2-carboxaldehyde-(2'-hydroxybenzoyl)hydrazone (**1b**)

Ligand **1b**, a yellow precipitate, was obtained from equimolar amounts of 8-hydroxyquinoline-2-carboxaldehyde and 2-hydroxybenzoylhydrazine as the preparation of ligand **1a**. Yield: 81.0%; m.p. = 245–247 °C; ESI-MS m/z 308.2 $[M + H]^+$; 1H NMR (DMSO- d_6 , 200 MHz, TMS) δ : 8.621 (s, 1 H, 11-CH=N), 8.356 (d, $J = 8.6$ Hz, 1 H, 4-CH), 8.113 (d, $J = 8.6$ Hz, 1 H, 3-CH), 7.871 (d, 1 H, $J = 7.8$ Hz, 20-CH), 7.469–7.395 (m, 3 H, 5,6,18-CH), 7.133 (d, $J = 7.0$ Hz, 1 H, 7-CH), 7.018–6.943 (m, 2 H, 17,19-CH); IR (KBr): (cm^{-1}): 3464, 3250, 1643, 1607, 1532, 1288; UV-Vis (DMF/H₂O): λ_{max} (ϵ) = 294 (31600), 329 nm (23,600 $M^{-1} cm^{-1}$).

5.3.3. 8-hydroxyquinoline-2-carboxaldehyde-(4'-hydroxybenzoyl)hydrazone (**1c**)

Ligand **1c**, a pale yellow precipitate, was obtained from equimolar amounts of 8-hydroxyquinoline-2-carboxaldehyde and 4-hydroxybenzoylhydrazine as the preparation of ligand **1a**. Yield: 81.0%; m.p. = 279–280 °C; ESI-MS m/z 308.2 $[M + H]^+$; 1H NMR (DMSO- d_6 , 200 MHz, TMS) δ : 8.594 (s, 1 H, 11-CH=N), 8.329 (d, $J = 8.4$ Hz, 1 H, 4-CH), 8.088 (d, $J = 8.4$ Hz, 1 H, 3-CH), 7.834 (d, 2 H, $J = 10.4$ Hz, 16,20-CH), 7.493–7.379 (m, 2 H, 5,6-CH), 7.124 (d, $J = 6.8$ Hz, 1 H, 7-CH), 6.900 (d, $J = 10.4$ Hz, 2 H, 17,19-CH); IR (KBr): (cm^{-1}): 3320, 3139, 1660, 1632, 1581, 1277; UV-Vis (DMF/H₂O): λ_{max} (ϵ) = 300 (31,800), 326 nm (22,400 $M^{-1} cm^{-1}$).

5.3.4. 8-hydroxyquinoline-2-carboxaldehyde-(isonicotinyl)hydrazone (**1d**)

Ligand **1d**, a yellow precipitate, was also obtained from equimolar amounts of 8-hydroxyquinoline-2-carboxaldehyde and

isonicotinylhydrazine as the preparation of ligand **1a**. Yield: 71.0%; m.p. = 162–164 °C; ESI-MS m/z 293.2 $[M + H]^+$; 1H NMR (DMSO- d_6 , 200 MHz, TMS) δ : 8.813 (d, $J = 5.2$ Hz, 2 H, 17,19-CH), 8.657 (s, 1 H, 11-CH=N), 8.372 (d, $J = 8.8$ Hz, 1 H, 4-CH), 8.129 (d, $J = 8.8$ Hz, 1 H, 3-CH), 7.861 (d, $J = 5.2$ Hz, 2 H, 16,20-CH), 7.528–7.409 (m, 2 H, 5,6-CH), 7.148 (d, $J = 6.4$ Hz, 1 H, 7-CH); IR (KBr): (cm^{-1}): 3576, 3193, 1663, 1613, 1557, 1271; UV-Vis (DMF/H₂O): λ_{max} (ϵ) = 290 (28,600), 325 nm (17,800 $M^{-1} cm^{-1}$).

5.4. Preparation of the Dy(III) complexes

Complex **2a** was prepared by refluxing and stirring equimolar amounts of a 40 cm^3 methanol solution of ligand **1a** (0.058 g, 0.2 mmol) and Dy(NO₃) \cdot 6H₂O on a water-bath. After refluxed for 30 min, triethylamine (0.020 g, 0.2 mmol) was added into the reaction mixtures drop wise to deprotonate the phenolic hydroxyl substituent of 8-hydroxyquinolinato unit. Then, the mixtures were refluxed and stirred continuously for 8 h. After cooling to room temperature, the precipitate was centrifugalized, washed with methanol and dried in vacuum over 48 h to give an orange powder. Similarly, **2b**, **2c** and **2d** complexes were prepared from equimolar amounts of Dy(NO₃) \cdot 6H₂O and **1b**, **1c** and **1d**, respectively.

5.4.1. Complex **2a**

Yield: 88.3% (0.097 g); anal. calcd. for C₃₄H₃₀N₈O₁₄Dy₂: C 37.09, H 2.73, N 10.18, Dy 29.54; found: C 37.25, H 2.72, N 10.11, Dy 29.44; ESI-MS m/z 1321.2 $[M + H]^+$ (DMF solution); IR (KBr): (cm^{-1}): 3399, 1615, 1552, 1494, 1310, 1104, 1068, 936, 841, 740, 613, 563, 492; UV-Vis (DMF/H₂O): λ_{max} (ϵ) = 326 (41,600), 373 nm (32,100 $M^{-1} cm^{-1}$). Δm (DMF) = 38.8 $cm^2 \Omega^{-1} mol^{-1}$.

5.4.2. Complex **2b**

Yield: 87.1%; anal. calcd. for C₃₄H₃₀N₈O₁₆Dy₂: C 36.04, H 2.65, N 9.89, Dy 28.71; found: C 36.15, H 2.66, N 9.86, Dy 28.82; ESI-MS m/z 1353.2 $[M + H]^+$ (DMF solution); IR (KBr): (cm^{-1}): 3406, 3216, 1599, 1543, 1491, 1309, 1256, 1104, 1058, 922, 839, 761, 636, 585, 489; UV-Vis (DMF/H₂O): λ_{max} (ϵ) = 327 (29,400), 377 nm (29,900 $M^{-1} cm^{-1}$). Δm (DMF) = 36.0 $cm^2 \Omega^{-1} mol^{-1}$.

5.4.3. Complex **2c**

Yield: 92.8%; anal. calcd. for C₃₄H₃₀N₈O₁₆Dy₂: C 36.04, H 2.65, N 9.89, Dy 28.71; found: C 36.17, H 2.65, N 9.87, Dy 28.62; ESI-MS m/z 1353.2 $[M + H]^+$ (DMF solution); IR (KBr): (cm^{-1}): 3405, 3193, 1598, 1548, 1494, 1336, 1289, 1104, 1070, 926, 843, 741, 642, 564, 490; UV-Vis (DMF/H₂O): λ_{max} (ϵ) = 332 (42,700), 379 nm (37,300 $M^{-1} cm^{-1}$). Δm (DMF) = 38.9 $cm^2 \Omega^{-1} mol^{-1}$.

5.4.4. Complex **2d**

Yield: 85.8%; anal. calcd. for C₃₂H₂₈N₁₀O₁₄Dy₂: C 34.85, H 2.54, N 12.70, Dy 29.49; found: C 35.01, H 2.55, N 12.64, Dy 29.42; ESI-MS m/z 1323.2 $[M + H]^+$ (DMF solution); IR (KBr): (cm^{-1}): 3401, 1634, 1592, 1550, 1494, 1314, 1102, 1059, 935, 843, 740, 612, 566, 491; UV-Vis (DMF/H₂O): λ_{max} (ϵ) = 327 (44,900), 372 nm (36,600 $M^{-1} cm^{-1}$). Δm (DMF) = 34.9 $cm^2 \Omega^{-1} mol^{-1}$.

5.5. Determination of crystal structures

X-ray diffraction data for a crystal were performed with graphite-monochromated Mo $K\alpha$ radiation (0.71073 Å) on a Bruker APEX area-detector diffractometer and collected by the ω - 2θ scan technique at 273(2) K. The crystal structures were solved by direct methods. All non-hydrogen atoms were refined anisotropically by full-matrix least-squares methods on F^2 . A partial structure was obtained by direct methods and the remaining non-hydrogen atoms were located from difference maps. Hydrogen atoms were

located in geometrically defined positions and not refined. All calculations were performed using the programs SHELXS-97 and SHELXL-97 [62].

Acknowledgement

The study was supported by the National Natural Science Foundation of China (20475023) and Gansu NSF (3ZS 041-A25-016).

Appendix A. Supplementary data

CCDC 713869 (**2a**) and 713870 (**2b**) contain the supplementary crystallographic data for this paper. These data can be obtained free of charge from The Cambridge Crystallographic Data Centre via www.ccdc.cam.ac.uk/data_request/cif. Also can be found at, in the online version, doi:10.1016/j.ejmech.2009.09.015.

References

- [1] L.H. Schmidt, *Annu. Rev. Microbiol.* 23 (1969) 427.
- [2] A.A. El-Asmy, A.Z. El-Sonbati, A.A. Ba-Issa, M. Mounir, *Transit. Met. Chem.* 5 (1990) 222.
- [3] D. Parker, R.S. Dickins, H. Puschmann, C. Crossland, J.A.K. Howard, *Chem. Rev.* 102 (2002) 1977.
- [4] M. Albrecht, O. Osetska, R. Fröhlich, *Dalton Trans.* 23 (2005) 3757.
- [5] J.Z. Li, G. Li, W.J. Yu, *J. Chin. Rare Earth Soc.* 18 (2001) 71 (in Chinese).
- [6] Y.J. Ji, Z.H. Wang, J.L. Li, S.H. Peng, *J. Health Toxicol.* 8 (1994) 164 (in Chinese).
- [7] S.X. Liu, L. Wang, Y.Y. Liu, E.B. Wang, *J. Chin. Rare Earth Soc.* 15 (1997) 59 (in Chinese).
- [8] R.B. Hunter, W. Walker, *Nature* 178 (1956) 47.
- [9] H.X. Liu, X.T. Liu, J.F. Lu, R.C. Li, K. Wang, *J. Beijing Med. Univ.* 32 (2000) 203 (in Chinese).
- [10] D.M. Kramsch, A.J. Aspen, L.J. Rozler, *Science* 213 (1981) 1511.
- [11] E.M. Hodnett, P.D. Mooney, *J. Med. Chem.* 13 (1970) 786.
- [12] E.M. Hodnett, W.J. Dunn, *J. Med. Chem.* 15 (1972) 339.
- [13] Y.B. Zeng, N. Yang, W.S. Liu, N. Tang, *J. Inorg. Biochem.* 97 (2003) 258.
- [14] A.M. Pyle, T. Morii, J.K. Barton, *J. Am. Chem. Soc.* 112 (1990) 9432.
- [15] J.K. Barton, J.M. Goldberg, C.V. Kumar, N.J. Turro, *J. Am. Chem. Soc.* 108 (1986) 2081.
- [16] S. Mahadevan, M. Palaniandavar, *Inorg. Chim. Acta* 254 (1997) 291.
- [17] S.J. Lippar, *Acc. Chem. Res.* 11 (1978) 211.
- [18] S.M. Hech, *Acc. Chem. Res.* 19 (1986) 383.
- [19] B.N. Ames, M.K. Shigenaga, T.M. Hagen, *Proc. Natl. Acad. Sci. U.S.A.* 90 (1993) 7915.
- [20] A.A. Horton, S. Fairhurst, *Crit. Rev. Toxicol.* 18 (1987) 27.
- [21] H.L. Wang, Z.Y. Yang, B.D. Wang, *Transit. Met. Chem.* 31 (2006) 470.
- [22] S.F. Lo, V. Mulabagal, C.L. Chen, C.L. Kuo, H.S. Tsay, *J. Agric. Food Chem.* 52 (2004) 6916.
- [23] S.Y. Chiang, J. Welch, F.J. Rauscher, T.A. Beerman, *Biochemistry* 33 (1994) 7033.
- [24] J.M. Woynarowski, M. Mchugh, R.D. Sigmund, T.A. Beerman, *Mol. Pharmacol.* 35 (1989) 177.
- [25] A.Y. Chen, C. Yu, B. Gatto, L.F. Liu, *Proc. Natl. Acad. Sci. U.S.A.* 90 (1993) 8131.
- [26] W.J. Geary, *Coord. Chem. Rev.* 7 (1971) 81.
- [27] M.M. Moawad, W.G. Hanna, *J. Coord. Chem.* 55 (2002) 439.
- [28] T.M.A. Ismail, *J. Coord. Chem.* 58 (2005) 141.
- [29] J.M. Ou-Yang, *J. Inorg. Chem.* 13 (1997) 315 (in Chinese).
- [30] X.H. Lu, Q.Y. Lin, L.C. Kong, X.Q. He, *Chem. Res. Appl.* 18 (2006) 1380 (in Chinese).
- [31] D. Suh, J.B. Chaires, *Bioorg. Med. Chem.* 3 (1995) 723.
- [32] R. Palchaudhuri, P.J. Hergenrother, *Curr. Opin. Biotechnol.* 18 (2007) 497.
- [33] S. Satyanarayana, J.C. Dabrowiak, J.B. Chaires, *Biochemistry* 31 (1992) 9319.
- [34] B.D. Wang, Z.Y. Yang, P. Crewdson, D.Q. Wang, *J. Inorg. Biochem.* 101 (2007) 1492.
- [35] R.D. Snyder, *Mutat. Res.* 623 (2007) 72.
- [36] J.K. Barton, A.T. Danishefsky, J.M. Goldberg, *J. Am. Chem. Soc.* 106 (1984) 2172.
- [37] H.L. Lu, J.J. Liang, Z.Z. Zeng, P.X. Xi, X.H. Liu, F.J. Chen, Z.H. Xu, *Transit. Met. Chem.* 32 (2007) 564.
- [38] C. Behrens, N. Harrit, P.E. Nielsen, *Bioconjugate Chem.* 12 (2001) 1021.
- [39] S. Frau, J. Bernadou, B. Meunier, *Bioconjugate Chem.* 8 (1997) 222.
- [40] D.S. Sigman, A. Mazumder, D.M. Perrin, *Chem. Rev.* 93 (1993) 2295.
- [41] Y. Wang, Z.Y. Yang, Q. Wang, Q.K. Cai, K.B. Yu, *J. Org. Chem.* 690 (2005) 4557.
- [42] J.Z. Wu, B.H. Ye, L. Wang, L.N. Ji, J.Y. Zhou, R.H. Li, Z.Y. Zhou, *J. Chem. Soc., Dalton Trans.* 8 (1997) 1395.
- [43] Y.C. Liu, Z.Y. Yang, J. Du, X.J. Yao, R.X. Lei, X.D. Zheng, J.N. Liu, H.S. Hu, H. Li, *Chem. Pharm. Bull.* 56 (2008) 443.
- [44] Y.C. Liu, Z.Y. Yang, J. Du, X.J. Yao, R.X. Lei, X.D. Zheng, J.N. Liu, H.S. Hu, H. Li, *Immunobiology* 213 (2008) 651.
- [45] L.A. Bagatolli, S.C. Kivatinitz, G.D. Fidelio, *J. Pharm. Sci.* 85 (1996) 1131.
- [46] M.M. Yang, P. Yang, L.W. Zhang, *Chin. Sci. Bull.* 9 (1994) 31.
- [47] A. Ayar, B. Mercimek, *Process Biochem.* 41 (2006) 1553.
- [48] Z.L. Li, J.H. Chen, K.C. Zhang, M.L. Li, R.Q. Yu, *Sci. China Ser B Chem.* 11 (1991) 1193 (in Chinese).
- [49] G. Scatchard, *Ann. N.Y. Acad. Sci.* 51 (1949) 660.
- [50] L.M. Berezkhovskiy, I.V. Astafieva, C. Cardoso, *Anal. Biochem.* 308 (2002) 239.
- [51] J.B. Chaires, N. Dattagupta, D.M. Crothers, *Biochemistry* 21 (1982) 3933.
- [52] J.D. McGhee, P.H. von Hippel, *J. Mol. Biol.* 86 (1974) 469.
- [53] M. Baldini, M. Belicchi-Ferrari, F. Bisceglie, G. Pelosi, S. Pinelli, P. Tarasconi, *Inorg. Chem.* 42 (2003) 2049.
- [54] Y. Wang, Z.Y. Yang, Z.N. Chen, *Bioorg. Med. Chem. Lett.* 18 (2008) 298.
- [55] J.-I. Ueda, N. Saito, Y. Shimazu, T. Ozawa, *Arch. Biochem. Biophys.* 333 (1996) 377.
- [56] C.C. Winterbourn, *Biochem. J.* 198 (1981) 125.
- [57] R. Xing, H. Yu, S. Liu, W. Zhang, Q. Zhang, Z. Li, P. Li, *Bioorg. Med. Chem.* 13 (2005) 1387.
- [58] F. Zsila, Z. Bikádi, M. Simonyi, *Org. Biomol. Chem.* 2 (2004) 2902.
- [59] A.G. Krishna, D.V. Kumar, B.M. Khan, S.K. Rawal, K.N. Ganesh, *Biochim. Biophys. Acta* 1381 (1998) 104.
- [60] C.C. Winterbourn, *Biochem. J.* 182 (1979) 625.
- [61] Z.Y. Guo, R.E. X. S. Liu, H.H. Yu, P.B. Wang, C.P. Li, P.C. Li, *Bioorg. Med. Chem. Lett.* 15 (2005) 4600.
- [62] G.M. Sheldrick, *Acta Crystallogr. A* 46 (1990) 467.